The spin-1 and spin-3/2 model on a bilayer Bethe lattice with crystal field

2007 J. Phys.: Condens. Matter 19 376212

(http://iopscience.iop.org/0953-8984/19/37/376212)

IOP PUBLISHING JOURNAL OF PHYSICS: CONDENSED MATTER

J. Phys.: Condens. Matter **19** (2007) 376212 (20pp) doi:10.1088/0953-8984/19/37/376212

The spin-1 and spin-3/2 model on a bilayer Bethe lattice with crystal field

E Albayrak and S Yilmaz

Department of Physics, Erciyes University, 38039, Kayseri, Turkey

Received 21 May 2007, in final form 29 July 2007
Published 22 August 2007
Online at stacks.iop.org/JPhysCM/19/376212

Abstract

A bilayer Ising model consisting of two Bethe lattices, each of which is coupled with crystal fields of different strengths and each with a branching ratio of q Ising spins with one of the layers having only spin-1 and the other having only spin-3/2, is laid over the top of the other and the two layers are tied together via an interaction between the vertically aligned spins. After obtaining the ground-state (GS) phase diagrams on different possible planes depending on the given system parameters, the changes in the order-parameters and the free energy are investigated by use of the exact recursion relations in a pairwise approach to calculate the phase diagrams of the model. The ferromagnetic ordering in each of the layers and ferromagnetic or antiferromagnetic ordering of the adjacent nearest-neighbor (NN) spins of the layers are considered. The system presents both second- and first-order phase transitions. The lines of the first-order phase transitions end on either the stable or unstable tricritical points or at the isolated critical points. The model also displays one or two compensation temperatures when the bilinear interaction of the upper layer with spin-1 can compete with that of the lower layers with spin-3/2.

1. Introduction

Thin films of various magnetic layered structures or superlattices have been receiving intense attention lately [1]. They are made up of multiple layers of different magnetic materials, therefore there is a high potential for technological improvements in information storage and retrieval and in the synthesis of new magnets for a variety of applications [2] as well as also presenting some interesting novel magnetic properties such as giant magnetoresistance [3], surface magnetic anisotropy [4], enhanced surface magnetic moment [5] and surface magnetoelastic coupling [6].

The multilayered structures containing only spin-1 atoms have been studied for only a few cases: e.g. the exact recursion relations approach was followed for the cases without and with the crystal field interactions [7] on the bilayer Bethe lattice. Coupled ferromagnetic and antiferromagnetic thin film systems were studied with a Heisenberg-like Hamiltonian by the application of a two-spin mean-field theory and an in-plane magnetic reorientation as a function

of temperature [8]. The stochastic series expansion quantum Monte Carlo (MC) method was used to study thin ferromagnetic films described by a Heisenberg model including local anisotropies [9]. Ferromagnetic thin films with magnetic single-ion anisotropies were studied within the framework of the Schwinger bosonization Heisenberg model and two alternative bosonizations were discussed [10]. The effect of the transverse field on bulk melting and layering sublimation transitions of a Blume–Emery–Griffiths (BEG) model was studied using the mean field theory (MFT) [11]. The non-equilibrium magnetic domain structure of growing ultrathin ferromagnetic films with a realistic atomic structure was studied as a function of coverage and temperature by applying a kinetic MC method [12]. The magnetic order–disorder layering transitions were investigated under the effect of variable surface crystal field using the MFT [13]. The complete global phase diagram for a bilayer model, whose interactions are described by the BEG model, was studied by the cluster variational method within the pair approximation [14]. The order–disorder layering transitions of the Blume–Capel model were investigated using MC simulations in the presence of a variable crystal field [15]. The multilayered spin-3/2 systems have received less attention than for the case with spin-1, i.e. there are only two works that we can report: the two-layered model with competing interactions was studied by using the interfacial approximation on a square lattice [16] and the bilayer Bethe lattice consisting of spin-3/2 atoms was studied by using the exact recursion relations [17].

Furthermore, molecular-based magnetic materials with spontaneous magnetic moments have been receiving great interest for their potential applications such as in thermomagnetic recording and in devices [18]. It is believed that ferrimagnetic ordering plays a crucial role in some of these materials. They consist of two unequal magnetic moments, i.e. a bipartite lattice with spin-S and spin-σ or layered structures with alternatingly placed spin-S and spin-σ, i.e. mixed multilayer systems, $S \neq \sigma$, which interact antiferromagnetically, therefore their moments do not cancel each other at low temperatures except at the compensation temperatures (T_{comp}). At the compensation points it was found that some physical properties present a peculiar behavior. For instance, the coercive field (H_{c}) is strongly temperature dependent only in the vicinity of T_{comp} [19]. It is a maximum at T_{comp}, falling to a minimum below T_{comp}, before rising again at low temperatures. This peculiar temperature dependence of H_{c}, together with local heating by a focused laser beam, can be applied to attain a direct overwrite capability in magneto-optical media [20].

As a result, multi-layer systems consisting of different types of spins in each layer have also attracted a great deal of attention. Thus, for the case with spin-1/2 and spin-1 we can list some of the works as follows: an Ising superlattice, consisting of two ferromagnetic materials A and B, with L_a layers of diluted spins $S_a = 1/2$ and L_b layers of diluted spins $S_b = 1$ in an applied transverse field with antiferromagnetic interface coupling, was examined using the effective field theory (EFT) with a probability distribution [21]. Two works including the effects of the crystal field are: a trilayer system, with two mixed spin interfaces ($S_{\mathrm{A}} = 1/2$, $S_{\mathrm{B}} = 1$) for arbitrary concentration and varied partial film thickness, was investigated using the EFT [22]; and a ferromagnetic multilayer system, consisting of L layers of spin-1/2 A-atoms, L layers of spin-1 B-atoms and a disordered phase in between them characterized by a random arrangement of A- and B-atoms of $\mathrm{A}_p\mathrm{B}_{1-p}$ type and negative A–B coupling, were studied within the framework of the EFT [23].

The works for the case including only spin-1/2 and spin-3/2 atoms without a crystal field may be given as: ferrimagnetic Ising layers in an applied transverse field were examined by the use of EFT [24]; and the effects of an applied transverse magnetic field on the magnetic properties in a ferrimagnetic bilayer system with disordered interfaces were investigated by the use of the MFT [25]. Also, works including crystal field effects are: an amorphous bilayer

system consisting of two magnetic monolayers was studied by the use of the EFT [26]; a bilayer system with $(A)_2(A_pB_{1-p})_1(B)_2$, consisting periodically of two layers of spin-1/2 A atoms, two layers of spin-3/2 atoms and an interface with alloying type (A_pB_{1-p}) disorder, was examined by using the EFT [27]; a ferromagnetic multilayer system, consisting periodically of two layers of spin-1/2 A-atoms, two layers of spin-3/2 B-atoms and a disordered interface between them characterized by a random arrangement of A and B atoms of A_pB_{1-p} type and a negative A–B coupling, was investigated via the standard MFT [28]; and the phase diagrams of spin-1/2 Ising semi-infinite and film ferromagnets with spin-3/2 overlayers were investigated within the framework of the EFT [29].

Some studies which examine the works with spin-1/2 and spin-1 or spin-3/2 and including the crystal field effects are as follows: the critical behavior of an Ising multilayer system consisting of alternating spin-1/2 and spin-S ($S \geqslant 1/2$) magnetic layers was given within the cluster approximation introduced into the differential operator technique [30]; a general formulation for the magnetic properties of layered Ising-type systems A_2B_n composed of two amorphous and n crystalline layers was presented for spin-1/2 and spin-S systems [31]; a ferromagnetic or ferrimagnetic mixed Ising bilayer system with both spin-1/2 and spin-1 (or spin-3/2) in a transverse crystal field was examined by the use of the EFT with a probability distribution technique [32]; a bilayer model, made up of two magnetic monolayers ($S_A = 1/2$ and $S_B = 1$ or $3/2$) with different interaction constants coupled together in a transverse crystal field, was studied by the use of the EFT with correlations [33]; and a ferromagnetic amorphous bilayer system, consisting of two monolayers (A and B) with different spins ($S_A = 1/2$ and $S_B = 1/2, 1$) and different interaction constants coupled together with an interlayer coupling, was studied by the EFT [34].

Unfortunately, we were not able to find any works including spin-1 and spin-3/2 atoms for multilayer systems. Thus, in this study we consider the bilayer Bethe lattice with an upper layer containing only spin-1 atoms with bilinear interaction constant J_1 and crystal field D_1 and a lower layer consisting of only spin-3/2 atoms with bilinear interaction constant J_2 and crystal field D_2. Then the two layers are allowed to interact with a bilinear interaction constant J_3 between the adjacent NN spins of the layers. The exact solutions of the model were obtained by the use of the exact recursion relations in a pairwise approach on the Bethe lattice [7, 17, 35]. As a result, the bilinear interaction and crystal field effects on the phase diagrams of the model were obtained by studying the variations of the order-parameters and the free energy of the system. The GS phase diagrams were also obtained as a guide in obtaining stable solutions of the model.

We should also note that the magnetic properties of a small particle on a hexagonal lattice are studied, where the particle was described by a mixed-spin Ising model in which the σ and S-spins are distributed in concentric and hexagonal rings [36]. In this work they also cite the work of Chern *et al* [37], which reports some measurements of the compensation points and phase diagrams of Fe_3O_4/Mn_3O_4 superlattices, a system grown by deposition of alternate layers of Fe_3O_4 and Mn_3O_4 coupled antiferromagnetically. Similar experimental examples with this work may be extended further, but of course it may not be possible to find an experimental work with one-to-one correspondence.

We have organized the rest of the paper as follows. In section 2, the bilayer Ising model is introduced and then the ground-state phase diagrams are obtained and discussed. In section 3 we obtain the order-parameters and free energy of the system in terms of the recursion relations exactly. Besides the thermal variations of the magnetizations, the phase diagrams of the model are illustrated and discussed in detail on different planes for given values of the system parameters in section 4. Finally, in section 5 we give a brief summary and make some concluding remarks.

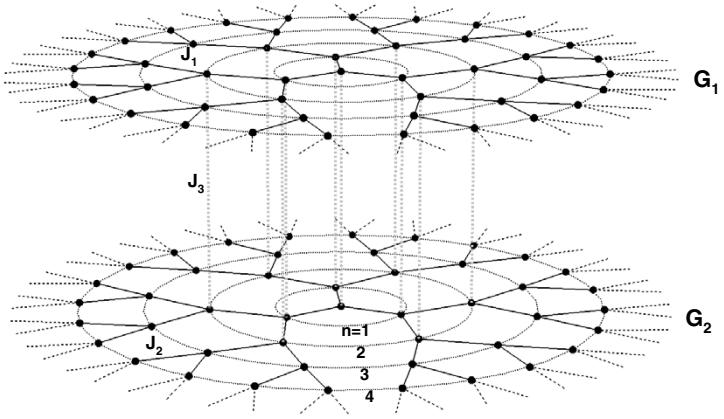

Figure 1. The bilayer Bethe lattice of coordination number $q = 3$. G_1 and G_2 refer to the upper and lower layers containing the spin-1 and spin-3/2 labeled as S_i and $\sigma_{i'}$, respectively. While J_1 and J_2 are the bilinear interactions of spins in G_1 and G_2, J_3 is the the bilinear interaction for the NN adjacent spins of G_1 and G_2.

2. Bilayer Bethe lattice and its ground states

The bilayer Bethe lattice is made up of two symmetrically placed layers of Bethe lattices, each of which has q NN Ising spins, i.e. coordination number, from its own layer and one adjacent NN spin from the other layer; thus, far from the boundaries that are deep inside the bilayer Bethe lattice, each spin has $q+1$ NNs in total, as shown in figure 1. The Hamiltonian, including the crystal fields and the NN bilinear spin interactions for the bilayer Bethe lattice, is given as

$$\mathcal{H} = -J_1 \sum_{\langle ij \rangle} S_i S_j - J_2 \sum_{\langle i' j' \rangle} \sigma_{i'} \sigma_{j'} - J_3 \sum_{\langle ii' \rangle} S_i \sigma_{i'} - D_1 \sum_i S_i^2 - D_2 \sum_{i'} \sigma_{i'}^2, \tag{1}$$

where S_i refers to spin-1 at site i with the values ± 1 and 0 on the upper layer G_1 and $\sigma_{i'}$ refers to spin-3/2 at site i' with the values $\pm 3/2$ and $\pm 1/2$ on the lower layer G_2. J_1 and J_2 are the intralayer bilinear interactions of the layers and the first and second summations run over all NN sites of G_1 and G_2, respectively. J_3 is the interlayer bilinear interaction of the adjacent NN spins between the layers G_1 and G_2, thus the third summation runs over all the adjacent neighboring sites of G_1 and G_2. D_1 and D_2 are the crystal field strengths coupled to the upper and lower layers, and thus the last two summations are over all the sites of G_1 and G_2, respectively.

In order to formulate the problem on the Bethe lattice, we need to introduce the order-parameters of the model. Thus, the spin-1 of the central pair from G_1 and spin-3/2 of the central pair from G_2 have magnetizations and quadrupolar order-parameters defined respectively as

$$m_1 = \langle S_0 \rangle \quad \text{and} \quad m_2 = \langle \sigma_{0'} \rangle, \quad Q_1 = \langle S_0^2 \rangle \quad \text{and} \quad Q_2 = \langle \sigma_{0'}^2 \rangle \tag{2}$$

where $\langle \cdots \rangle$ refers to the usual thermal average. Instead, one may equally use the total magnetization m, total quadrupolar moment Q and the staggered magnetization η, defined as

$$m = \tfrac{1}{2}(m_1 + m_2), \quad Q = \tfrac{1}{2}(Q_1 + Q_2) \quad \text{and} \quad \eta = \tfrac{1}{2}(m_1 - m_2). \tag{3}$$

The last order-parameter measures the correlations between the adjacent NN spins of the layers and is defined as

$$\rho = \langle S_0 \sigma_{0'} \rangle - \langle S_0 \rangle \langle \sigma_{0'} \rangle \tag{4}$$

which is called the spin–spin correlation function.

Table 1. Ground-state configurations for spin-1 and spin-3/2 model on the bilayer Bethe lattice. The phases are indicated with (S_0, S_1) and $(\sigma_{0'}, \sigma_{1'})$ NN pairs for the layers in G_1 and G_2 with ground-state values of spin-1 and spin-3/2, respectively.

I	$\pm1, \pm1$ $\pm\frac{3}{2}, \pm\frac{3}{2}$	II	$\pm1, \pm1$ $\mp\frac{3}{2}, \mp\frac{3}{2}$	III	$\pm1, \mp1$ $\pm\frac{3}{2}, \mp\frac{3}{2}$
IV	$\mp1, \pm1$ $\pm\frac{3}{2}, \mp\frac{3}{2}$	V	$\mp1, \mp1$ $\pm\frac{3}{2}, \mp\frac{3}{2}$	VI	$0, \mp1$ $\pm\frac{3}{2}, \mp\frac{3}{2}$
VII	$0, \mp1$ $\mp\frac{3}{2}, \pm\frac{3}{2}$	VIII	$\mp1, \mp1$ $\mp\frac{3}{2}, \mp\frac{1}{2}$	IX	$\mp1, \mp1$ $\pm\frac{1}{2}, \mp\frac{3}{2}$
X	$\mp1, \mp1$ $\pm\frac{3}{2}, \mp\frac{1}{2}$	XI	$\mp1, \mp1$ $\pm\frac{3}{2}, \pm\frac{1}{2}$	XII	$\mp1, \mp1$ $\mp\frac{1}{2}, \mp\frac{1}{2}$
XIII	$\mp1, \mp1$ $\mp\frac{1}{2}, \pm\frac{1}{2}$	XIV	$\mp1, \mp1$ $\pm\frac{1}{2}, \pm\frac{1}{2}$	XV	$0, 0$ $\mp\frac{3}{2}, \pm\frac{3}{2}$
XVI	$0, 0$ $\pm\frac{1}{2}, \mp\frac{1}{2}$	XVII	$0, 0$ $\mp\frac{1}{2}, \mp\frac{1}{2}$	XVIII	$0, 0$ $\mp\frac{3}{2}, \mp\frac{3}{2}$
XIX	$\mp1, \pm1$ $\mp\frac{1}{2}, \pm\frac{1}{2}$	XX	$0, \mp1$ $\mp\frac{3}{2}, \mp\frac{3}{2}$	XXI	$\mp1, \pm1$ $\pm\frac{1}{2}, \mp\frac{1}{2}$
XXII	$0, \mp1$ $\pm\frac{3}{2}, \pm\frac{3}{2}$				

In addition to the order-parameters, we also need the GS phase diagrams, to use them as a guide in obtaining stable solutions for the temperature-dependent phase diagrams of the model. In order to obtain the GS phase diagrams, we consider a central plaquette which consist of four NN pair spins of the bilayer system with one pair $\langle ij \rangle$ with spin-1 only on layer G_1, one pair $\langle i'j' \rangle$ with spin-3/2 only on layer G_2, and two pairs $\langle ii' \rangle$ and $\langle jj' \rangle$ connecting layers G_1 and G_2 between the two spin-1 and spin-3/2 pairs only. The GS phase diagrams were obtained by comparing the values of the energy for different spin configurations and then the GS configurations are those with the lowest energy for given values of the system parameters. As a result, we have obtained the following 22 different types of GS configurations from consideration of the central plaquette deep inside the bilayer Bethe lattice, as given in table 1.

In the GS phase diagrams the lines are the boundary lines separating the different types of phases, thus each line contains each of the phases that are involved in the separation and may be called the coexistence lines. The points at which these lines combine are the multiphase points, where all the allowed phases coexist. Thus the first GS phase diagrams are obtained on the $(J_2/|J_1|, J_3/q|J_1|)$ plane for arbitrarily given values of $D/q|J_1|$, i.e. $D = D_1 = D_2$, and are presented in figures 2$((i)$–$(v))$. In figure 2(i) for $D/q|J_1| \geqslant 0$, we see that the system only presents the configurations I–V, i.e. ferromagnetic, ferrimagnetic, mixed, antiferromagnetic and surface ferromagnetic phases, respectively. We obtain the same GS phase diagrams for zero and all positive values of the crystal field, which means that the crystal field has no effect on the model when it is positive. But, for negative values of the crystal field, the GS phase diagrams change drastically. For $D/q|J_1| < 0$, the multiphase lines are split by the new configurations. These new configurations are seen at higher ground-state energies as the $D/q|J_1|$ becomes more and more negative. Figure 2(ii) is obtained for $D/q|J_1| = -0.25$, which presents the new configurations VI–XIV compared with the previous figure. Thus it is obvious that the magnetizations of the layers are never zero, since only one of the spins in layer G_1 prefers to be in the spin-0 state; see table 1. But when $D/q|J_1| = -0.5$, as depicted in figure 2(iii), we see that the configurations V, IX, X and XIII of figure 2(ii) have

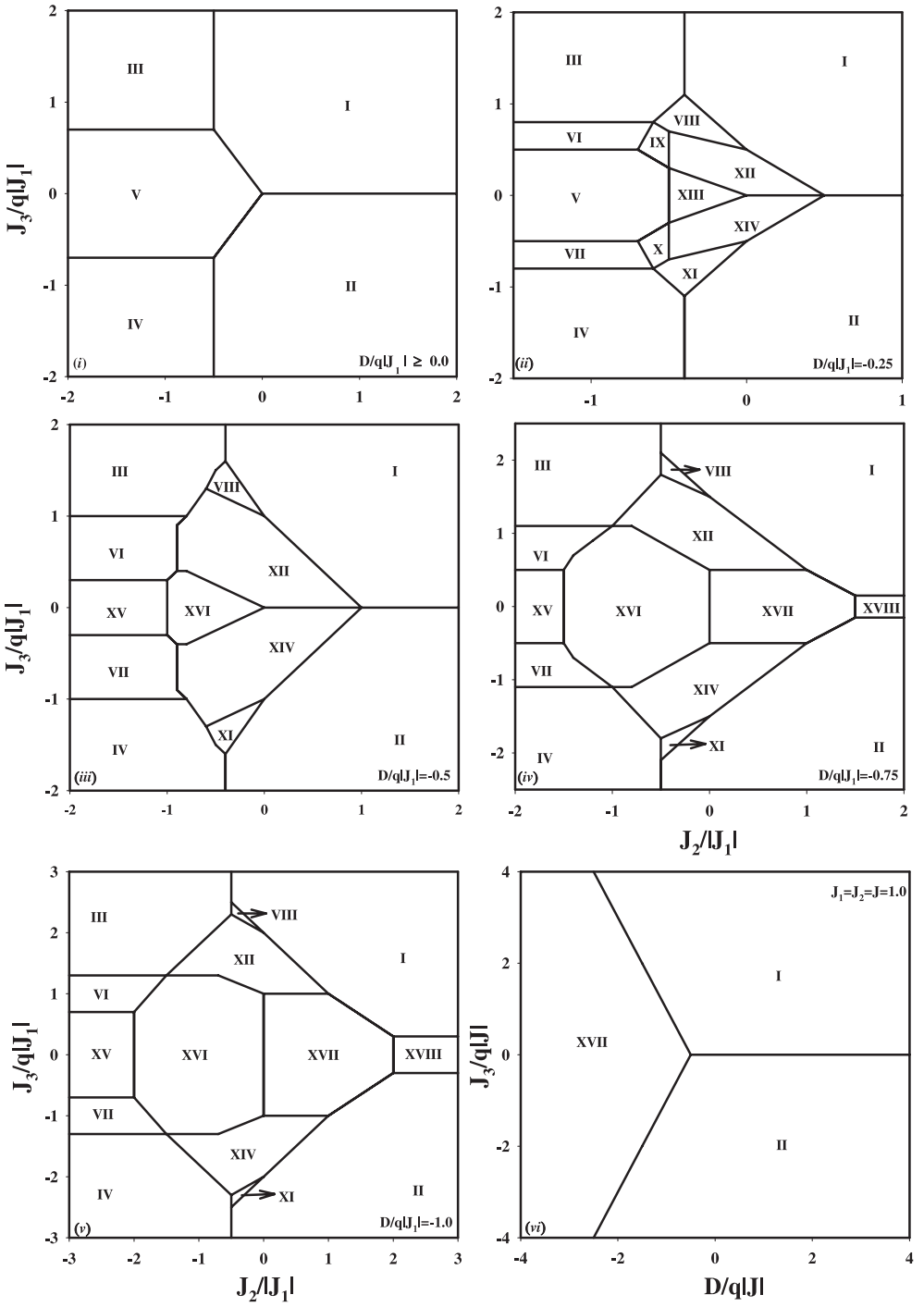

Figure 2. The ground-state phase diagrams: on the $(J_2/|J_1|, J_3/q|J_1|)$ planes for (i) $D/q|J_1| \geqslant 0$, (ii) $D/q|J_1| = -0.25$, (iii) $D/q|J_1| = -0.5$, (iv) $D/q|J_1| = -0.75$ and (v) $D/q|J_1| = -1.0$; (vi) on the $(D/q|J|, J_3/q|J|)$ plane for $J_1 = J_2 = J = 1.0$; (vii) on the $(D_1/q|J|, D_2/q|J|)$ plane for $J_1 = J_2 = J = 1.0$ and $J_3/q|J| = 1.0$; $(viii)$ on the $(qJ/|J_3|, D/|J_3|)$ plane for $J_1 = J_2 = J = 1.0$ $J_3/q|J| = 1.0$; and (ix) on the $(qJ_2/|J_3|, qJ_1/|J_3|)$ plane for $D/|J_3| = -1.0$ and $J_3 = 1.0$.

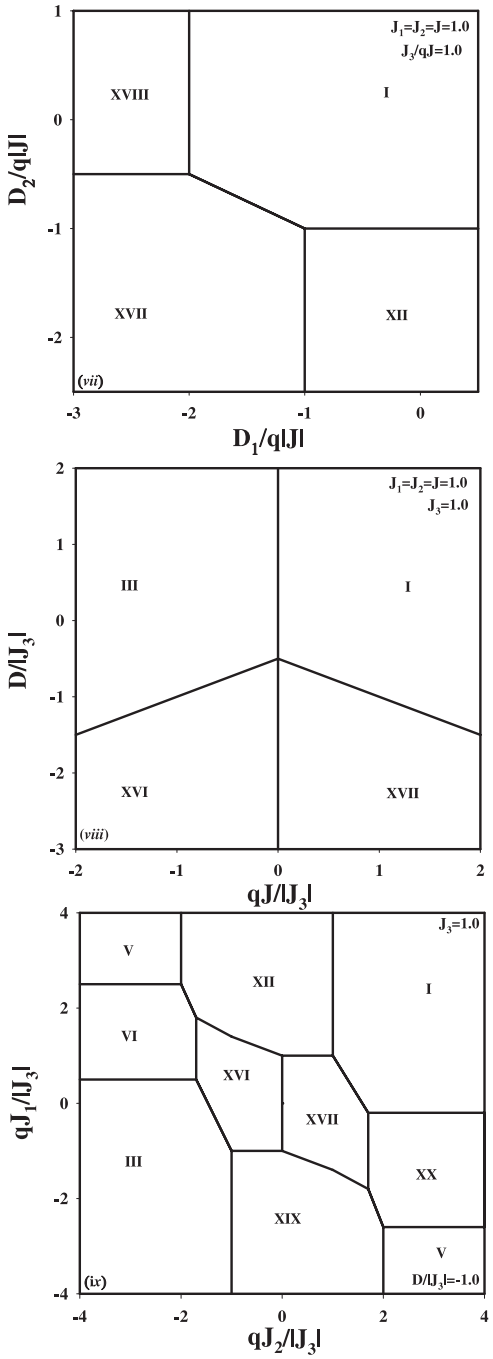

Figure 2. (Continued.)

disappeared, but instead the configurations XV and XVI appear, for which the magnetization of the layers vanishes, since both spin-1 in layer G_1 prefer to be in the spin-0 state and the layer G_2 is in the antiferromagnetic configuration (so the total magnetization becomes zero).

Figure 2(*iv*) illustrates the GS phase diagram when $D/q|J_1|$ is set equal to -0.75, which shows that the multiphase lines separating the phases XII and XIV and I and II of figure 2(*iii*) are split by the new configurations XVII and XVIII, respectively. It is clear from figure 2(*v*) that, as $D/q|J_1|$ becomes more negative, neither the configurations nor the patterns of the configurations change, but the areas covered by them increase. Figure 2(*vi*) illustrates the phase diagram on the $(D/q|J|, J_3/q|J|)$ plane for $J_1 = J_2 = J = 1.0$, where we see that the model only presents the phases I, II and XVII. This may be caused by the reduction in the number of system parameters by one with the condition $J_1 = J_2 = J$. The next GS phase diagrams are presented on the $(D_1/q|J|, D_2/q|J|)$ plane for $J_1 = J_2 = J = 1.0$ when $J_3/qJ = 1.0$ in figure 2(*vii*). It should be mentioned that the phases I and XII of figure 2(*vii*) are replaced by the phases II and XIV, respectively, with a sign change of J_3. But the two phases XVII and XVIII remain unchanged with a sign change of J_3, since the spins of the upper layer are in the spin-0 state. Figure 2(*viii*) is obtained for $J_1 = J_2 = J$ when $J_3 = 1$ on the $(qJ/|J_3|, D/|J_3|)$ plane. For this, phases I and III when $J_3 = 1$ are exchanged with phases II and IV, respectively, with a sign change of J_3, as expected. But the phases XVI and XVII remain unchanged again, since the spins of the upper layer are in the spin-0 state. The final GS phase diagram is obtained on the $(qJ_2/|J_3|, qJ_1/|J_3|)$ plane for $D/|J_3| = -1.0$ when $J_3 = 1$. Note that the sign change of J_3 causes phases I, III, VI, XII, XIX and XX of this figure 2(*ix*) to be exchanged with phases II, IV, VII, XIV, XXI and XXII, respectively. But the phases V, XVI and XVII remain unchanged in both figures. It should be noted that the GS phase diagrams are used to obtain the stable solutions and configurations of the temperature-dependent phase diagrams, which will be examined in section 4.

3. The system parameters in terms of the recursion relations

In order to obtain the exact recursion relations on the bilayer Bethe lattice, one has to start with a calculation of the partition function of the model. In the calculation, we assume that the adjacent NN spins of G_1 and G_2 containing one spin-1 and one spin-3/2 are considered as pairs; see figure 1. The first pair deep inside the bilayer lattice is called the central pair, which forms the first-generation spins. This central pair of spins is connected by q NN spin pairs, i.e. the coordination number, which forms the second-generation spins. Each pair of spins in the second generation is joined to $(q-1)$ NNs. Therefore, in total the second generation has $q(q-1)$ NNs which form the third generation, and so on to infinity [7, 17, 35]. Thus each spin far from the boundaries has $(q+1)$ NN spins: q spins from the layer to which it belongs, i.e. with same type of spin, and one from the adjacent layer, i.e. with the other type of spin.

The usual definition of the partition function is given as

$$Z = \sum_{\text{All Config.}} \mathrm{e}^{-\beta\mathcal{H}} = \sum_{\text{Spc}} P(\text{Spc}), \tag{5}$$

and it is calculated in a recursive approach on the bilayer Bethe lattice by using the Ising Hamiltonian, i.e. equation (1). The $P(\text{Spc})$ may be considered as an unnormalized probability distribution over the spin configurations (Spc). Starting from the central pair of spins on the Bethe lattice made up of q separate branches connecting each of the pair of spins, one follows only one of the branches of the tree out of q, therefore for the full formulation we have to define the partition function for each of these separate branches named $g_n(S, \sigma)$. It should be mentioned that each spin S_i with spin-1 can take the values ± 1 and 0, and each spin $\sigma_{i'}$ with spin-3/2 can take the values $\pm 3/2$ and $\pm 1/2$, thus we have to define 12 $g_n(S, \sigma)$ functions for $3 \times 4 = 12$ configurations for each pair of spins at their sites. Thus in this pairwise approach [7, 17, 35], 11 exact recursion relations are defined as the ratios of these partition

functions of the separate branches on the bilayer Bethe lattice, and are given as

$$\begin{aligned}
A_n &= \frac{g_n(1,\frac{3}{2})}{g_n(-1,\frac{-1}{2})}, \qquad B_n = \frac{g_n(1,\frac{1}{2})}{g_n(-1,\frac{-1}{2})}, \qquad C_n = \frac{g_n(1,\frac{-1}{2})}{g_n(-1,\frac{-1}{2})},\\
D_n &= \frac{g_n(1,\frac{-3}{2})}{g_n(-1,\frac{-1}{2})}, \qquad E_n = \frac{g_n(0,\frac{3}{2})}{g_n(-1,\frac{-1}{2})}, \qquad F_n = \frac{g_n(0,\frac{1}{2})}{g_n(-1,\frac{-1}{2})},\\
G_n &= \frac{g_n(0,\frac{-1}{2})}{g_n(-1,\frac{-1}{2})}, \qquad H_n = \frac{g_n(0,\frac{-3}{2})}{g_n(-1,\frac{-1}{2})}, \qquad I_n = \frac{g_n(-1,\frac{3}{2})}{g_n(-1,\frac{-1}{2})},\\
J_n &= \frac{g_n(-1,\frac{1}{2})}{g_n(-1,\frac{-1}{2})}, \qquad K_n = \frac{g_n(-1,\frac{-3}{2})}{g_n(-1,\frac{-1}{2})},
\end{aligned} \tag{6}$$

where each recursion relation is a function of the recursion relations for the NN shell with $(n-1)$, therefore they are totally nonlinear in their nature. In order to obtain their numerical values for given system parameters, numerical methods were to be employed. Note also that the choice of what ratios of these $g_n(S,\sigma)$ functions is to be taken is totally arbitrary. In the thermodynamic limit ($n \to \infty$) these recursion relations determine the states of the system, therefore they may be called the equations of state. Unfortunately, the explicit formulations of the recursion relations are too long to be given here.

Now we can obtain the order-parameters of the model in terms of these recursion relations. Thus, the magnetizations and quadrupolar moments are calculated in terms of the recursion relations for layer G_1 with spin-1 of the central pair as

$$\begin{aligned}
M_1 = \langle S_0 \rangle = [&\mathrm{e}^{\beta(\frac{3}{2}J_3+D_1+\frac{9}{4}D_2)}A_n^q + \mathrm{e}^{\beta(\frac{1}{2}J_3+D_1+\frac{1}{4}D_2)}B_n^q\\
&+ \mathrm{e}^{\beta(-\frac{1}{2}J_3+D_1+\frac{1}{4}D_2)}C_n^q + \mathrm{e}^{\beta(-\frac{3}{2}J_3+D_1+\frac{9}{4}D_2)}D_n^q - \mathrm{e}^{\beta(-\frac{3}{2}J_3+D_1+\frac{9}{4}D_2)}I_n^q\\
&- \mathrm{e}^{\beta(-\frac{1}{2}J_3+D_1+\frac{1}{4}D_2)}J_n^q - \mathrm{e}^{\beta(\frac{3}{2}J_3+D_1+\frac{9}{4}D_2)}K_n^q - \mathrm{e}^{\beta(\frac{1}{2}J_3+D_1+\frac{1}{4}D_2)}]/\Delta_1
\end{aligned} \tag{7}$$

and

$$\begin{aligned}
Q_1 = \langle S_0^2 \rangle = [&\mathrm{e}^{\beta(\frac{3}{2}J_3+D_1+\frac{9}{4}D_2)}A_n^q + \mathrm{e}^{\beta(\frac{1}{2}J_3+D_1+\frac{1}{4}D_2)}B_n^q\\
&+ \mathrm{e}^{\beta(-\frac{1}{2}J_3+D_1+\frac{1}{4}D_2)}C_n^q + \mathrm{e}^{\beta(-\frac{3}{2}J_3+D_1+\frac{9}{4}D_2)}D_n^q + \mathrm{e}^{\beta(-\frac{3}{2}J_3+D_1+\frac{9}{4}D_2)}I_n^q\\
&+ \mathrm{e}^{\beta(-\frac{1}{2}J_3+D_1+\frac{1}{4}D_2)}J_n^q + \mathrm{e}^{\beta(\frac{3}{2}J_3+D_1+\frac{9}{4}D_2)}K_n^q + \mathrm{e}^{\beta(\frac{1}{2}J_3+D_1+\frac{1}{4}D_2)}]/\Delta_1,
\end{aligned} \tag{8}$$

and for layer G_2 with spin-3/2 of the central pair as

$$\begin{aligned}
M_2 = \langle \sigma_{0'} \rangle = [&3\mathrm{e}^{\beta(\frac{3}{2}J_3+D_1+\frac{9}{4}D_2)}A_n^q + \mathrm{e}^{\beta(\frac{1}{2}J_3+D_1+\frac{1}{4}D_2)}B_n^q\\
&- \mathrm{e}^{\beta(-\frac{1}{2}J_3+D_1+\frac{1}{4}D_2)}C_n^q - 3\mathrm{e}^{\beta(-\frac{3}{2}J_3+D_1+\frac{9}{4}D_2)}D_n^q + 3\mathrm{e}^{\frac{9}{4}\beta D_2}E_n^q + \mathrm{e}^{\frac{1}{4}\beta D_2}F_n^q\\
&- \mathrm{e}^{\frac{1}{4}\beta D_2}G_n^q - 3\mathrm{e}^{\frac{9}{4}\beta D_2}H_n^q + 3\mathrm{e}^{\beta(-\frac{3}{2}J_3+D_1+\frac{9}{4}D_2)}I_n^q + \mathrm{e}^{\beta(-\frac{1}{2}J_3+D_1+\frac{1}{4}D_2)}J_n^q\\
&- 3\mathrm{e}^{\beta(\frac{3}{2}J_3+D_1+\frac{9}{4}D_2)}K_n^q - \mathrm{e}^{\beta(\frac{1}{2}J_3+D_1+\frac{1}{4}D_2)}]/2\Delta_1
\end{aligned} \tag{9}$$

and

$$\begin{aligned}
Q_2 = \langle \sigma_{0'}^2 \rangle = [&9\mathrm{e}^{\beta(\frac{3}{2}J_3+D_1+\frac{9}{4}D_2)}A_n^q + \mathrm{e}^{\beta(\frac{1}{2}J_3+D_1+\frac{1}{4}D_2)}B_n^q\\
&+ \mathrm{e}^{\beta(-\frac{1}{2}J_3+D_1+\frac{1}{4}D_2)}C_n^q + 9\mathrm{e}^{\beta(-\frac{3}{2}J_3+D_1+\frac{9}{4}D_2)}D_n^q + 9\mathrm{e}^{\frac{9}{4}\beta D_2}E_n^q + \mathrm{e}^{\frac{1}{4}\beta D_2}F_n^q\\
&+ \mathrm{e}^{\frac{1}{4}\beta D_2}G_n^q + 9\mathrm{e}^{\frac{9}{4}\beta D_2}H_n^q + 9\mathrm{e}^{\beta(-\frac{3}{2}J_3+D_1+\frac{9}{4}D_2)}I_n^q + \mathrm{e}^{\beta(-\frac{1}{2}J_3+D_1+\frac{1}{4}D_2)}J_n^q\\
&+ 9\mathrm{e}^{\beta(\frac{3}{2}J_3+D_1+\frac{9}{4}D_2)}K_n^q + \mathrm{e}^{\beta(\frac{1}{2}J_3+D_1+\frac{1}{4}D_2)}]/4\Delta_1,
\end{aligned} \tag{10}$$

respectively. Δ_1 is the partition function, obtained from equation (5) in terms of the recursion relations as

$$\begin{aligned}\Delta_1 = {} & \mathrm{e}^{\beta(\frac{3}{2}J_3+D_1+\frac{9}{4}D_2)}A_n^q + \mathrm{e}^{\beta(\frac{1}{2}J_3+D_1+\frac{1}{4}D_2)}B_n^q \\ & + \mathrm{e}^{\beta(-\frac{1}{2}J_3+D_1+\frac{1}{4}D_2)}C_n^q + \mathrm{e}^{\beta(-\frac{3}{2}J_3+D_1+\frac{9}{4}D_2)}D_n^q + \mathrm{e}^{\frac{9}{4}\beta D_2}E_n^q + \mathrm{e}^{\frac{1}{4}\beta D_2}F_n^q \\ & + \mathrm{e}^{\frac{1}{4}\beta D_2}G_n^q + \mathrm{e}^{\frac{9}{4}\beta D_2}H_n^q + \mathrm{e}^{\beta(-\frac{3}{2}J_3+D_1+\frac{9}{4}D_2)}I_n^q + \mathrm{e}^{\beta(-\frac{1}{2}J_3+D_1+\frac{1}{4}D_2)}J_n^q \\ & + \mathrm{e}^{\beta(\frac{3}{2}J_3+D_1+\frac{9}{4}D_2)}K_n^q + \mathrm{e}^{\beta(\frac{1}{2}J_3+D_1+\frac{1}{4}D_2)}. \end{aligned} \tag{11}$$

The last order-parameter is the spin–spin correlation function between the adjacent NN spins of the central pair of two layers, and is expressed by

$$\begin{aligned}\rho = {} & [3\mathrm{e}^{\beta(\frac{3}{2}J_3+D_1+\frac{9}{4}D_2)}A_n^q + \mathrm{e}^{\beta(\frac{1}{2}J_3+D_1+\frac{1}{4}D_2)}B_n^q - \mathrm{e}^{\beta(-\frac{1}{2}J_3+D_1+\frac{1}{4}D_2)}C_n^q \\ & - 3\mathrm{e}^{\beta(-\frac{3}{2}J_3+D_1+\frac{9}{4}D_2)}D_n^q - 3\mathrm{e}^{\beta(-\frac{3}{2}J_3+D_1+\frac{9}{4}D_2)}I_n^q - \mathrm{e}^{\beta(-\frac{1}{2}J_3+D_1+\frac{1}{4}D_2)}J_n^q \\ & + 3\mathrm{e}^{\beta(\frac{3}{2}J_3+D_1+\frac{9}{4}D_2)}K_n^q + \mathrm{e}^{\beta(\frac{1}{2}J_3+D_1+\frac{1}{4}D_2)}]/2\Delta_1 - \langle S_0\rangle\langle\sigma_{0'}\rangle. \end{aligned} \tag{12}$$

In addition to the order-parameters, one also needs the free energy in terms of the recursion relations to obtain the stable solutions of the model. The free-energy expression on the Bethe lattice has already been obtained for the case with only one spin per lattice site [38], but it can easily be generalized to our case. Hence, the free energy of a homogeneous phase of the bilayer Bethe lattice is given as

$$-\beta F = \frac{2-q}{2}\ln(\Delta_1) + \frac{q}{2}\ln(\Delta_2) \tag{13}$$

where

$$\begin{aligned}\Delta_2 = {} & \mathrm{e}^{\beta(-J_1-\frac{3}{4}J_2+\frac{3}{2}J_3+D_1+\frac{9}{4}D_2)}A_{n-1}^{q-1} + \mathrm{e}^{\beta(-J_1-\frac{1}{4}J_2+\frac{1}{2}J_3+D_1+\frac{1}{4}D_2)}B_{n-1}^{q-1} \\ & + \mathrm{e}^{\beta(-J_1+\frac{1}{4}J_2-\frac{1}{2}J_3+D_1+\frac{1}{4}D_2)}C_{n-1}^{q-1} + \mathrm{e}^{\beta(-J_1+\frac{3}{4}J_2-\frac{3}{2}J_3+D_1+\frac{9}{4}D_2)}D_{n-1}^{q-1} \\ & + \mathrm{e}^{\beta(-\frac{3}{4}J_2+\frac{9}{4}D_2)}E_{n-1}^{q-1} + \mathrm{e}^{\beta(-\frac{1}{4}J_2+\frac{1}{4}D_2)}F_{n-1}^{q-1} + \mathrm{e}^{\beta(\frac{1}{4}J_2+\frac{1}{4}D_2)}G_{n-1}^{q-1} \\ & + \mathrm{e}^{\beta(\frac{3}{4}J_2+\frac{9}{4}D_2)}H_{n-1}^{q-1} + \mathrm{e}^{\beta(J_1-\frac{3}{4}J_2-\frac{3}{2}J_3+D_1+\frac{9}{4}D_2)}I_{n-1}^{q-1} \\ & + \mathrm{e}^{\beta(J_1-\frac{1}{4}J_2-\frac{1}{2}J_3+D_1+\frac{1}{4}D_2)}J_{n-1}^{q-1} + \mathrm{e}^{\beta(J_1+\frac{3}{4}J_2+\frac{3}{2}J_3+D_1+\frac{9}{4}D_2)}K_{n-1}^{q-1} \\ & + \mathrm{e}^{\beta(J_1+\frac{1}{4}J_2+\frac{1}{2}J_3+D_1+\frac{1}{4}D_2)}. \end{aligned} \tag{14}$$

The obtained free-energy values for given system parameters are used to find the places of the first-order phase transition temperatures and the stable solutions of the model. We should also note that, in order to obtain the behaviors of the order-parameters and the free energy, first the recursion relations are calculated by using an iteration scheme, then the values of the recursion relations that are found are inserted into the definitions of the order-parameters and the free energy, which are functions of the interlayer and intralayer bilinear interactions, the crystal fields coupled to the layers, and the coordination number q. Detailed phase diagrams of the model are obtained from a study of the variations in the order-parameters and free energy in the guidance of the GS phase diagrams, and are given in the next section.

4. Variations of the system parameters and phase diagrams

The critical temperatures and their behaviors were studied to obtain the phase diagrams of the model for the case with only $J_1 > 0$ and $J_2 > 0$, ferromagnetic couplings in layers G_1 and G_2, and $J_3 > 0$ or $J_3 < 0$, ferromagnetic or antiferromagnetic coupling between the layers, respectively, including the effects of the crystal fields of the layers. Note that in the rest of this work we use the term temperature, T, in place of the reduced temperature kT/J_i, with $i = 1$ or with no subscript when $J_1 = J_2 = J_3$.

Before going on to study the phase diagrams, first we have searched for the existence of an important phenomenon, i.e. the compensation. The compensation temperature, $T_{\rm comp}$, can be located by finding the crossing point between the absolute values of the layer magnetizations,

$$|M_1(T_{\rm comp})| = |M_2(T_{\rm comp})| \tag{15}$$

or when the net magnetization goes to zero

$$M_{\rm NET} = |M_1(T_{\rm comp})| - |M_2(T_{\rm comp})| = 0 \tag{16}$$

with the conditions

$$\text{sign}[M_2(T_{\rm comp})] = -\text{sign}[M_1(T_{\rm comp})], \qquad T_{\rm comp} < T_{\rm c}. \tag{17}$$

These conditions ensure that at $T_{\rm comp}$ the two layer magnetizations cancel each other, whereas at the second-order phase transition temperature, $T_{\rm c}$, both layer magnetizations and the net magnetization go to zero. Thus we have obtained that the model presents one or two compensations, depending on the values of the system parameters. Figure 3(a) shows the existence of only one compensation for $J_2/J_1 = 0.1$, $J_3/J_1 = 0.2$ and $D_1/J_1 = D_2/J_1 = 9.0$. The compensation temperature $T_{\rm comp} \simeq 0.696$ and the second-order phase transition temperature $T_{\rm c} \simeq 1.89$, where $T_{\rm comp} < T_{\rm c}$, as expected. The inset of the figure shows the effect of changing the J_3/J_1 values and illustrates that, as J_3/J_1 values increase, the $T_{\rm comp}$ increases and gets closer to the $T_{\rm c}$ values. Figure 3(b) presents the existence of two compensations for $J_2/J_1 = J_3/J_1 = 1.0$, $D_1/J_1 = 2.0$ and $D_2/J_1 = -1.25$. The first compensation is seen at higher values of magnetization and at a lower temperature, $T_{\rm comp1} \simeq 0.966$, and the second one is seen at lower values of magnetization and at a higher temperature $T_{\rm comp2} \simeq 1.742$, where $T_{\rm c} = 2.478$ (the inset presents the D_1/J_1 variations of the compensations). In addition, the thermal variations of magnetization are also studied to present a few points clearly for $J_3 = 0$, i.e. in that case we have two non-interacting single-layered Bethe lattices. As the spin values become lower, the order–disorder temperatures are seen at lower temperatures when $J_1 = J_2$, i.e. spin-1 has a lower order–disorder temperature than spin-3/2, which persists until some critical value of J_2 of spin-3/2. At this critical value, the magnetizations of both the layers go to zero together at the same order–disorder temperature, and below which the layer with higher spin goes to zero temperature before the layer with lower spin and when the layer magnetizations can compensate each other before the magnetizations go to zero. In the figures, we present the layer magnetizations, m_1 and m_2, the total magnetization m and the staggered magnetization η (the absolute value of η is used to show the existence of the compensation temperatures). Figure 3(c) is obtained for $D/qJ_1 = 3.0$, $J_2/J_1 = 1.0$ and $J_3 = 0.0$, and it is clear that the order–disorder temperature, or the second-order phase transition temperature, of m_1 is $T_{\rm c1}$, which acts as the first-order phase transition temperature, $T_{\rm t}$, of m and η. After these temperatures, the system is driven by the lower layer with spin-3/2, since above these temperatures the upper layer with spin-1 remains disordered. This means that above $T_{\rm c1}$, the system jumps to the order–disorder temperatures, $T_{\rm c2}$, of the lower layer with spin-3/2, and in between there is a gap where no critical temperatures exist. The $T_{\rm c}$ temperatures of the layers become equal at some critical value of J_2/J_1, below which the magnetization of the lower layer becomes zero before the upper layer. Thus, when $J_2/J_1 = 0.1$, the roles of the layers changes (see figure 3(d)). In this case the lower layer with higher spin presents its order–disorder temperature before the upper layer with lower spin, since J_2 is less than its critical value, $T_{\rm c2} < T_{\rm c1}$. Now $T_{\rm c2}$s act as the $T_{\rm t}$ temperatures of m and η. Afterwards, the system jumps to the critical values of the upper layer, and in between there is a gap with no critical temperatures. Note also that the system can only compensate when J_2 is less than its critical values.

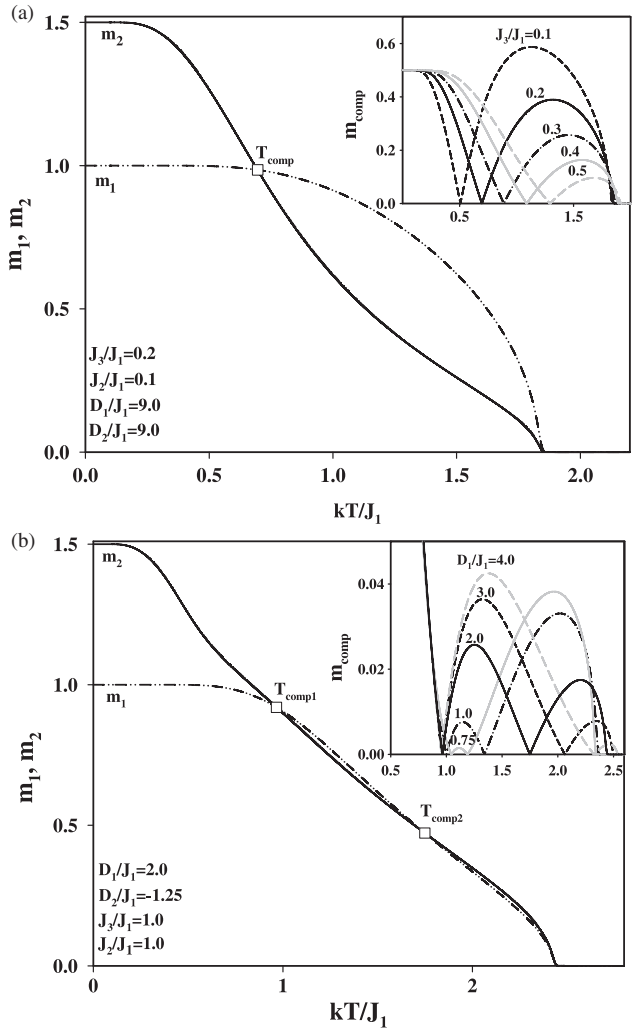

Figure 3. The thermal variations of m_1, m_2 and $m_{\rm comp} = |m_1 - m_2|$: (*a*) showing only one compensation, with the compensation temperature $T_{\rm comp}$ indicated by a square, for $J_3/J_1 = 0.2$, $J_2/J_1 = 0.1$ and $D_1/J_1 = D_2/J_1 = 9.0$; (*b*) showing two compensations for $J_3/J_1 = J_2/J_1 = 1.0$ and $D_1/J_1 = 2.0$ and $D_2/J_1 = -1.25$. The thermal variations of m_1, m_2, m and $|\eta|$ for $J_3/J_1 = 0.0$; (*c*) showing that the $T_{\rm c1}$ of m_1 acts as the $T_{\rm t}$ of m and $|\eta|$ with $T_{\rm c2} > T_{\rm c1}$ for $D/qJ_1 = 3.0$ and $J_2/J_1 = 1.0$; and (*d*) showing that the $T_{\rm c2}$ of m_2 acts as the $T_{\rm t}$ of m and $|\eta|$ with $T_{\rm c1} > T_{\rm c2}$ for $D/qJ_1 = 3.0$ and $J_2/J_1 = 0.1$.

We are now ready to obtain the phase diagrams of our model on some of the possible planes, depending on the given system parameters in the light of the GS phase diagrams for $q = 3$ corresponding to the honeycomb lattice. In the phase diagrams, the second- and first-order phase transition temperature lines and the lines of the compensation temperatures are indicated by solid, dashed and gray dotted-dashed lines, respectively. The filled (•) circles and the empty circles (○) indicate the tricritical (TCP) and isolated critical points, respectively. Meanwhile, the values of the quadrupole moments are used to distinguish the P_+ and P_- phases of the paramagnetic phase corresponding to the (*i*) $m = 0$, $Q > 23/24$, and (*ii*) $m = 0$, $Q < 23/24$, respectively, and the boundaries in between them are indicated by dotted lines.

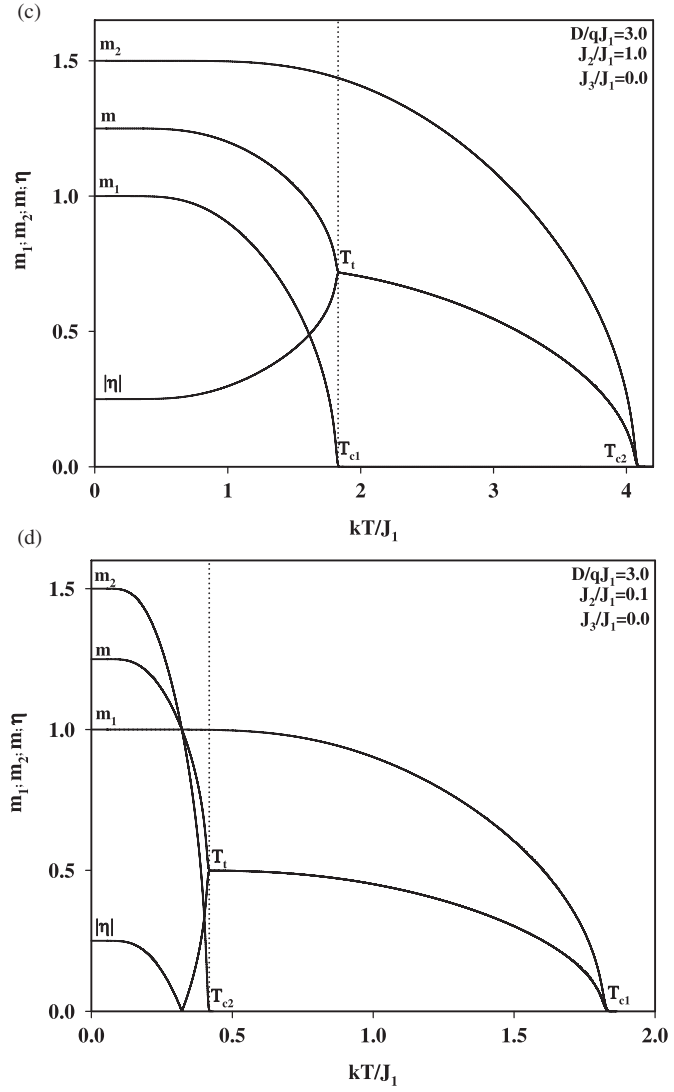

Figure 3. (Continued.)

The first phase diagram is obtained on the $(kT/J_1, J_3/J_1)$ plane to show the effect of changing J_2/J_1, i.e. for the values of 0.1, 0.25, 0.35, 0.6 and 1.0, for equal values of the crystal fields, $D/qJ_1 = 1.0$, for the layers; see figure 4(a). As can be seen, phases I and II are separated by T_t-lines at low temperatures which continue until the (○)s for each given J_2/J_1 value along $J_3/J_1 = 0$. Then, above these (○)s, the system jumps to the T_c temperatures of either the lower layer or the upper layer, depending on the competition between J_1 and J_2 values and where a triple point (TP) is formed. Thus the crossed lines along $J_3 = 0$ are the lines of no transitions between the (○)s and the TPs for a given J_2/J_1. At the TPs, three phases I, II and P_+ coexist together and, where the T_c-lines separate into two symmetrical wings, i.e while the upper T_c-line separates the phases I and P_+ corresponding to $J_3/J_1 > 0$, the lower one separates the phases II and P_+ corresponding to the $J_3/J_1 < 0$. As $|J_3/J_1| \to \infty$, these wings become constant at $kT/J_1 \simeq 2.27, 2.89, 3.3, 4.33$ and 5.98 for a given J_2/J_1 in the above order. It

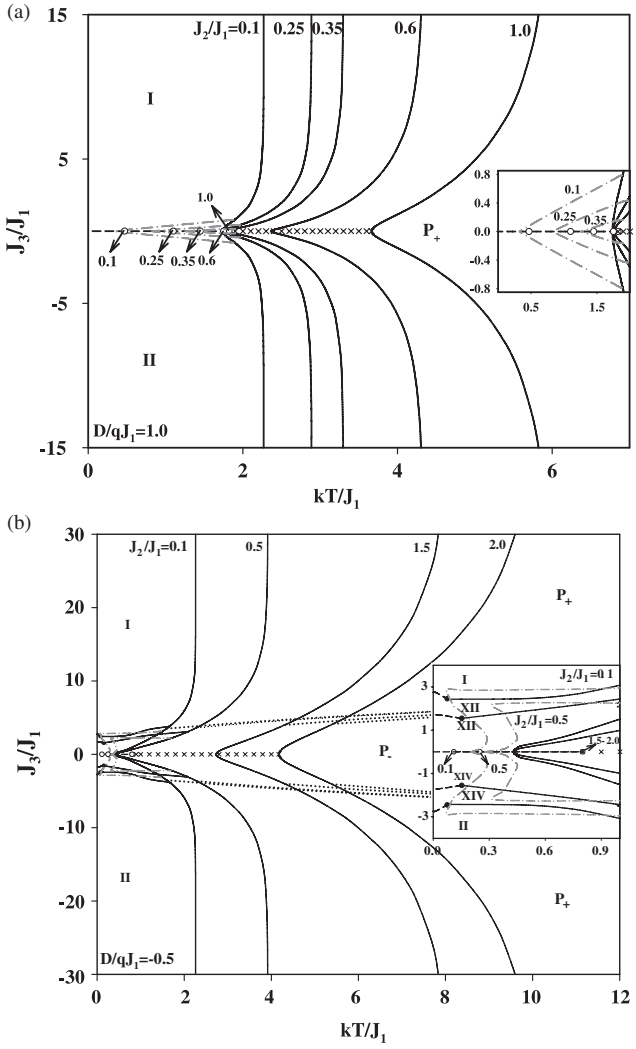

Figure 4. The phase diagrams on the $(kT/J_1, J_3/J_1)$ planes for (a) $D/qJ_1 = 1.0$ and $J_2/J_1 = 0.1, 0.25, 0.35, 0.6, 1.0$; (b) $D/qJ_1 = -0.5$ and $J_2/J_1 = 0.1, 0.5, 1.5, 2.0$; (c) $D/qJ_1 = -1.0$ and $J_2/J_1 = 0.1$; (d) $D/qJ_1 = -1.0$ and $J_2/J_1 = 1.5, 2.5, 3.5$.

is clear that, as J_2/J_1 decreases, the P_+ phase pushes the T_c-lines to lower temperatures, increasing the disorder in the system. The $(\circ)$ temperatures corresponding to J_2/J_1 values are about 0.47, 1.1, 1.45, 1.75 and 1.82, respectively. As the J_2/J_1 values decrease, the $(\circ)$ points appear at lower temperatures. The system presents compensation temperatures for $J_2/J_1 = 0.1, 0.25$ and 0.35. These are found by taking the absolute values of m (η) in the region with the phase II (I), respectively. Thus, for each value of J_2/J_1, two symmetrical branches of compensation lines emerging from the same temperature are found. As the temperature increases, these branches move linearly to higher $|J_3/J_1|$ values and eventually end on the corresponding T_c-lines. It is clear that, for lower values of J_2, the system exhibits compensation temperatures, since then J_1 of spin-1 can compete with J_2 of spin-3/2.

For negative values of the crystal fields, the phase diagrams change drastically at low temperatures. According to the GS phase diagram in figure 2(iii), figure 4(b) presents such

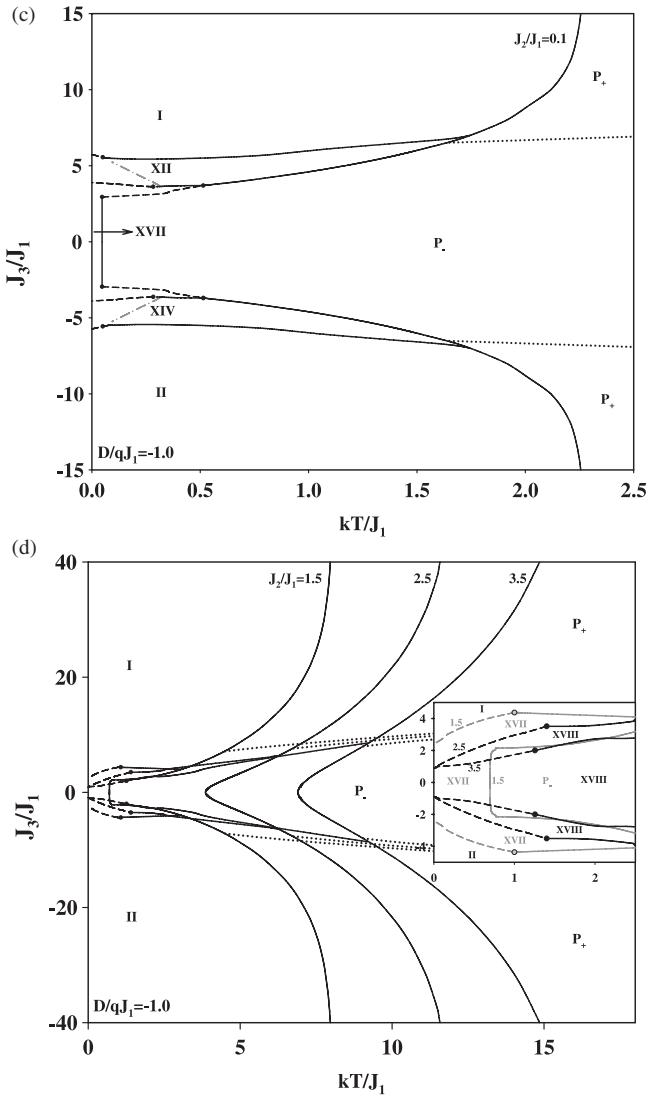

Figure 4. (Continued.)

a phase diagram again on the $(kT/J_1, J_3/J_1)$ plane for $J_2/J_1 = 0.1$, 0.5, 1.5 and 2.0 when $D/qJ_1 = -0.5$. Besides the T_t-lines similar to those (i.e. ending on the (○)s) in figure 4(a) along $J_3/J_1 = 0$, two more symmetrical T_t-lines when $J_3/J_1 \neq 0$ for $J_2/J_1 = 0.1$ and 0.5 are obtained, as seen in figure 4(b). These two symmetrical lines continue until the (●) points, from which two symmetrical T_c-lines emerge. Then these lines end on the corresponding wing-shaped T_c-lines. These combinations of the T_t- and T_c-lines separate the phases I and XII when $J_3/J_1 > 0$ and the phases XIV and II when $J_3/J_1 < 0$. The phases XII and XIV for $J_3/J_1 = 0$ are separated by the T_t-lines ending at the (○)s. The behaviors of the critical lines for $J_2/J_1 = 1.5$ and 2.0 remain qualitatively unchanged in comparison with the previous figure. Again, the crossed lines along $J_3/J_1 = 0$ correspond to the lines of no transitions between the (○)s and TPs. We have found that the system exhibits compensation temperatures for $J_2/J_1 = 0.1$ and 0.5. Two symmetrical branches of T_{comp}-lines emerge from $J_3/J_1 = 0$-

axis; actually, they form a shape that looks like the upper part of the human lips. Then, from the lowest part of this line, part of the roughly linear $T_{\rm comp}$-lines emerges for each $J_2/J_1 = 0.1$ and 0.5. It is obvious that the $T_{\rm comp}$-lines are seen in the regions of the ordered phases. In addition, two symmetrical branches of the phase boundary lines separating the P_+ and P_- phases appear on the $T_{\rm c}$-lines, which spreads very slowly as the temperature increases.

The phase diagrams, as presented in figures 4(c) and (d), were obtained from consideration of the GS phase diagram in figure 2(v). In figure 4(c), obtained for $J_2/J_1 = 0.1$ and $D/qJ_1 = -1.0$, one expects two pairs of symmetrical $T_{\rm t}$-lines at $kT/J_1 = 0$ according to the GS phase diagrams. Thus the first pair of $T_{\rm t}$-lines are seen at higher J_3/J_1, i.e. at about ± 5.703, which end on the (•) points from where two symmetrical $T_{\rm c}$-lines come out. We see that these $T_{\rm c}$-lines combine with other symmetrical $T_{\rm c}$-lines at a higher temperature. The second pair of $T_{\rm t}$-lines is seen at lower $J_3/J_1 \simeq \pm 3.9$, which end on the higher (•) point temperatures from where the symmetrical $T_{\rm c}$-lines appear again. As we mentioned above, these $T_{\rm c}$-lines combine with the previous ones and, as $|J_3/J_1| \to \infty$, they become constant at a temperature of about 2.27. A second $T_{\rm c}$-line with a vertical portion connects the second pair of $T_{\rm t}$-lines at a lower temperature. Note also that the first pair of critical lines separates the phases I and XII from above and II and XIV from below. The second pair separates the phases XII and XVII from above and XIV and XVII from below at very low temperatures, but they are separated by the P_- phase afterwards. Two symmetrical compensation lines also appear in the phase regions XII and XIV. Figure 4(d) was calculated for $J_2/J_1 = 1.5, 2.5$ and 3.5 and $D/qJ_1 = -1.0$. For $J_2/J_1 = 1.5$, one has to go through the phases II, XVII and I, while for $J_2/J_1 = 2.5$ and 3.5 the phases II, XVIII and I have to be crossed according to figure 2(v). Thus, in order to distinguish these phases and the critical lines in the phase diagrams, we have indicated them in gray for $J_2/J_1 = 1.5$. As can be seen, two symmetrical $T_{\rm t}$-lines appear at zero temperature which end on the corresponding (•) points and again, from them, two symmetrical $T_{\rm c}$-lines emerge for each J_2/J_1 value. Eventually, they all connect with the corresponding wing-shaped $T_{\rm c}$-line, which has a vertical section for $J_2/J_1 = 1.5$ in comparison with the others. As can be seen, the upper part of the critical lines for $J_2/J_1 = 1.5$ separates the phases I and XVII and the lower part separates the phases II and XVII below the lowest temperature of the wing-shaped $T_{\rm c}$-line, and with P_- afterwards. For $J_2/J_1 = 2.5$ and 3.5, the phase XVII is exchanged with XVIII in comparison to the case with $J_2/J_1 = 1.5$. Again, the dotted lines are the boundary lines separating the phases P_- and P_+.

Figures 5(a) and (b) were obtained on the $(kT/J, J_3/J)$ and $(D/J, kT/J)$ planes for given values D/qJ and J_3/J, respectively, when $J_1 = J_2 = J$ by using figure 2(vi). In figure 5(a), the phase diagram for $D/qJ = -1.0$ is almost the same as that in figure 4(d) when $J_2/J_1 = 1.5$, i.e. even the critical lines separate the same phases. When $D/qJ = -0.6$, the system presents first a $T_{\rm t}$-line starting from zero temperature, which is then separated into two symmetrical $T_{\rm t}$-lines at a temperature about $kT/J = 0.16$, then the rest of its behavior is qualitatively similar to previous case, i.e. when $D/qJ = -1.0$. For the zero and positive values of D/qJ, i.e. 0.0, 0.5, 2.5 and 5.0, the critical lines are also qualitatively similar to those in figure 4(a). For these values of D/qJ, we did not find any compensations. The (P) phase is divided into the P_+ and P_- phases for $D/qJ = -1.0$ and -0.6, that is, the exterior and the interior regions of the dotted lines are the P_+ and P_- phases, respectively, and this only consists of the P_+ phase for $D/qJ = 0.0$, 0.5, 2.5 and 5.0. Note also that the wing-shaped $T_{\rm c}$-lines coincide and become constant at a temperature of about 5.98 for all D/qJ values. In figure 5(b), the $T_{\rm c}$-lines start at a temperature of about 0.469 for all values of J_3/J. As the crystal field values increase, the $T_{\rm c}$ temperatures of these lines also increase sharply at first, but as the D/J values increase further they become constant at some temperatures. These temperatures are observed at higher values, for higher value of J_3/J. Besides, the system also

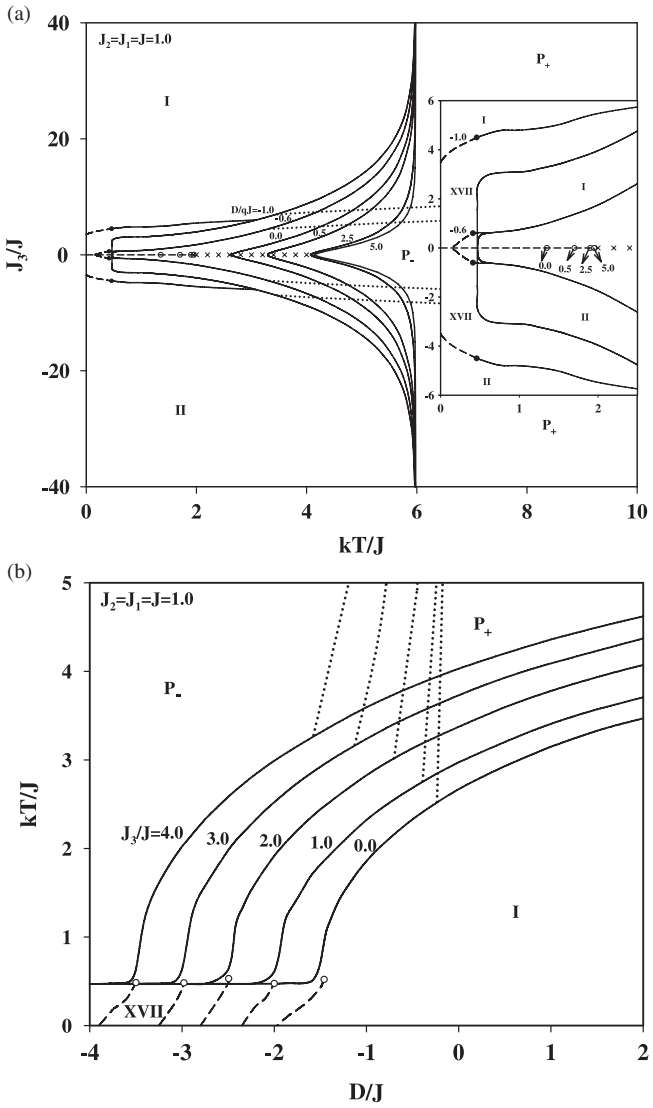

Figure 5. The phase diagrams on the (a) $(kT/J, J_3/J)$ and (b) $(D/J, kT/J)$ planes for given D/qJ and J_3/J values, respectively.

exhibits T_t-lines separating the phases XVII and I for all values of J_3/J. These lines end at isolated critical points indicated by (○). The P_- and P_+ phases are separated by boundary lines starting from the T_c-lines for each J_3/J. Below the joints between the boundary lines and the T_c-lines, the P_- and I phases and the above P_+ and I phases are separated by T_c-lines.

Our final two phase diagrams are obtained on the $(D_i/J, kT/J)$ planes for given D_j/J, $i \neq j$, when $J_1 = J_2 = J$ and $J_3/qJ = 1.0$ with $i = 1, 2$. The first one is given in figure 6(a) with $i = 1$ and for given D_2/J values. The upper inset shows that T_c-lines starting from different temperatures as $D_1/J \to -\infty$ for $D_2/J = 0.0, -0.75$ and -1.2 are not very interesting, since they do not present any critical points along them. These lines separate the paramagnetic phases from phases I and XVIII at high and low D_1/J values, respectively. The boundary lines separating P_- and P_+ phases and the T_t-lines ending at the isolated critical

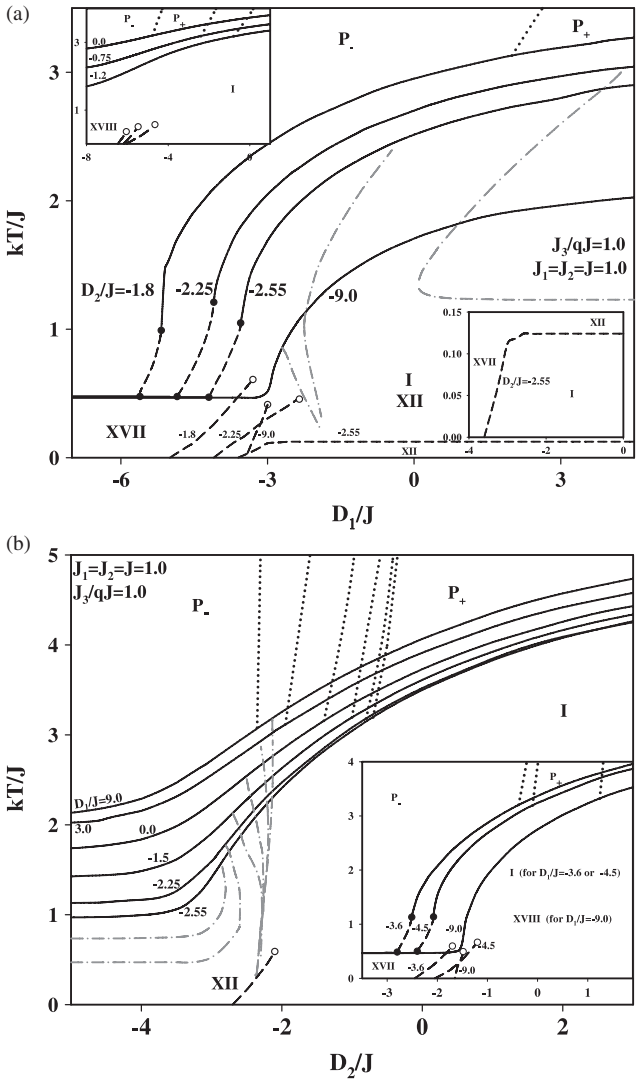

Figure 6. The phase diagrams on the (*a*) $(D_1/J, kT/J)$ and (*b*) $(D_2/J, kT/J)$ planes for given D_2/J and D_1/J values, respectively.

points are also found, and these show similar behaviors to those in the previous figure. Note also that these T_t-lines separate the phases I and XVIII at low temperatures. But in the main figure, the behaviors of the T_c-lines present new behaviors; they start from the same temperature, i.e. $kT/J = 0.475$, as $D_1/J \to -\infty$ but, as D_1/J increases, they suddenly exhibit tricritical points along the same temperature at $D_1/J = -5.61$, -4.85 and -4.2 for $D_2/J = -1.8$, -2.25 and -2.55, respectively. These first TCP points are the unstable ones, as will be clear in a while. The T_t-lines emerge from these unstable TCP points for each $D_2/J = -1.8$, -2.25 and -2.55, and then they end on the second TCP points, but now they are stable since their free energies are lower in comparison with the previous ones. The second T_c-lines emerge from these stable TCP points and, as the temperature increases, they also increase gradually, and as $D_1/J \to \infty$, they become constant at some temperature. When

$D_2/J = -9.0$ we see that these TCP points and the portion of the T_t-lines between them disappear, i.e. its behavior is the same as those in the upper inset. We have also found that the T_t-lines end at the isolated critical points for $D_2/J = -1.8$, -2.25 and -9.0, but for $D_2/J = -2.55$ the T_t-line does not present an isolated critical point, i.e. it is continuous at $kT/J = 0.124$. Note also that the T_t-lines for $D_2/J = -1.8$ and -2.25 separate the phases I and XVII, and for $D_2/J = -9.0$ it separates the phases XII and XVII, but for $D_2/J = -2.55$ the continuous T_t-line separates the phases XVII and I at low D_1/J and separates the phases XII and I at higher D_1/J (see lower inset). The boundary lines separating the P_- and P_+ phases move towards the right, i.e. to higher values of D_1/J, as D_2/J becomes more negative. The compensation lines emerge from their corresponding T_c-lines and are seen to move to lower D_1/J values as D_2/J becomes more negative. The next and final phase diagram, figure 6(b), was obtained on the $(D_2/J, kT/J)$ plane for a given D_1/J. The behaviors of the T_c-lines for $D_1/J = 9.0$, 3.0, 0.0, -1.5, -2.25 and -2.55 are similar to those presented in the upper inset of the previous figure. The T_t-lines for these values of D_1/J lie along the same points, end on the same isolated critical points, and separate the phases XII and I. The compensation lines emerge from their corresponding T_c-lines at higher temperatures, and they combine at lower temperature and terminate for $D_1/J = 9.0$, 3.0, 0.0 and -1.5, but they make a U-turn towards the left for $D_1/J = -2.25$ and -2.55 and, as $D_2/J \to -\infty$, they become continuous at some constant temperatures. In the inset we see that the system presents unstable and stable TCPs and isolated critical points for $D_1/J = -3.6$ and -4.5, as in figure 6(a) for $D_2/J = -1.8$ and -2.25. The T_t-lines separate the phases XVII and I. When $D_1/J = -9.0$, we again see similar qualitative behaviors, as for $D_2/J = -9.0$ in the previous figure, but now the T_t-line separates the phases XVII and XVIII. The boundary lines separating P_- and P_+ phases also show similar behaviors as in the previous figure. It should be noted that, while the ground-state phase diagrams are exact, the temperature-dependent phase diagrams are calculated by using numerical techniques, therefore there may have been some discrepancies from the ground-state values.

5. Summary and conclusions

In this work we have analyzed a bilayer Ising model consisting of two Bethe lattices interacting with an interlayer bilinear interaction, each of which is coupled with crystal fields and intralayer bilinear interactions of different strengths, each with a branching ratio of q Ising spins with one of the layers having only spin-1 and the other having only spin-3/2. The GS phase diagrams are obtained exactly on different possible planes, depending on the given interaction parameters. As a result, it was found that the GS phase diagrams remain qualitatively the same when $D/qJ_1 \geqslant 0$ and when $D/qJ_1 \leqslant -0.75$, but they present differences in the transition region, i.e. between these values of D/qJ_1. The GS configurations when $D/qJ_1 < 0$ correspond to higher-energy configurations than $D/qJ_1 \geqslant 0$ and also, as D/qJ_1 becomes more negative, the disorder in the configurations increases at low J_3/J_1 and J_2/J_1 values. The model presents either first- or second-order phase transitions. The T_t-lines ending at the (○)s along $J_3/J_1 = 0$ split into two symmetrical lines as D/qJ_1 becomes more negative, and end on the (●)s. We see that, starting from the (○)s up to the TP along $J_3/J_1 = 0$, there are lines of no transition, indicated by the crossed lines for each given value of the system parameters. The T_c-lines emerging from the two symmetrical (●)s end on the corresponding wing-shaped T_c-lines. The finding that the system presents either stable or unstable (●)s, decided by comparing their free energies, is also observed in the mixed spin-1 and spin-3/2 Ising models on a single-layered Bethe [39] and on the honeycomb lattice [40]. The wing-shaped T_c-lines are also observed in works where the effects of the interlayer exchange interaction J_{inter} in coupled Co/Cu/Ni trilayers was studied, as motivated by experiments in [8], where they found an overall

agreement with experimental results, and the work which investigated the phase transitions in a bilayer lattice gas [41] modeled analogously similar to this work.

As a last word, we should note that it is really unfortunate for us not to be able to compare our results directly with similar works. We hope that this work will lead others to study similar systems by using different techniques.

References

[1] Elmers H J 1995 *Int. J. Mod. Phys.* B **9** 3115
[2] *Digest 13th Int. Colloq. on Magnetic Films and Surfaces (Glasgow)* 1991
[3] Baibich M N, Broto J M, Fert A, Nguyen Van Dau F, Petroff F, Eitenne P, Creuzet G, Friederich A and Chazelas J 1988 *Phys. Rev. Lett.* **61** 2472
Binasch G, Grunberg P, Saurenbach F and Zinn W 1989 *Phys. Rev.* B 4828
[4] Sayama J, Asahi T, Mizutani K and Osaka T 2004 *J. Phys. D: Appl. Phys.* **37** L1–4
[5] Wu R and Freeman A J 1992 *Phys. Rev.* B **45** 7205
Donath M 1999 *J. Phys.: Condens. Matter* **11** 9421
[6] O'Handley R C and Sun S W 1991 *Phys. Rev. Lett.* **66** 2798
Bochi G, Song O and O'Handley R C 1994 *Phys. Rev.* B **50** 2043
[7] Albayrak E and Canko O 2007 *Physcia* A **373** 363
Canko O and Albayrak E 2007 *Phys. Rev.* E **75** 011116
[8] Jensen P J and Dreysse H 2002 *Phys. Rev.* B **66** 220407
[9] Henelius P, Fröbrich P, Kuntz P J, Timm C and Jensen P J 2002 *Phys. Rev.* B **66** 094407
[10] Timm C and Jensen P J 2000 *Phys. Rev.* B **62** 5634
[11] Benyoussef A, Ez-Zahraouy H, Mahboub H and Quazzani M J 2003 *Physica* A **326** 220
[12] Brinzanik R, Jensen P J and Bennemann K H 2002 *J. Magn. Magn. Mater.* **238** 258
[13] Bahmad L, Benyoussef A and Ez-Zahraouy H 2002 *J. Magn. Magn. Mater.* **251** 115
[14] Tucker J W, Balcerzak T, Gzik M and Sukiennicki A 1998 *J. Magn. Magn. Mater.* **187** 381
[15] Bahmad L, Benyoussef A and Ez-Zahraouy H 2004 *M. J. Condens. Matter* **5** 134
Bahmad L, Benyoussef A and Ez-Zahraouy H 2004 *Surf. Sci.* **552** 1
[16] Horiguchi T, Lipowski A and Tsushima N 1996 *Physica* A **224** 626
[17] Albayrak E, Yilmaz S and Akkaya S 2007 *J. Magn. Magn. Mater.* **310** 98
[18] Gatteshi D, Khan O, Miller J S and Palacio F (ed) 1991 *Magnetic Molecular Materials* (*NATO ASI Series*) (Dordrecht: Kluwer–Academic)
Khan O 1993 *Molecular Magnetism* (New York: VCH)
[19] Shieh H P D and Kryder M H 1986 *Appl. Phys. Lett.* **49** 473
Connel G A N, Allen R and Mansuripur M 1982 *J. Appl. Phys.* **53** 7759
Ostorero J, Escorne M, Guegan A P, Soulette F and Le Gall H 1994 *J. Appl. Phys.* **75** 6103
[20] Williams H J, Sherwood R C, Foster F G and Kelley E M 1957 *J. Appl. Phys.* **28** 1181
[21] Oubelkacem A, El Aouad N, Benaboud A and Saber M 2004 *J. Magn. Magn. Mater.* **279** 299
[22] Wiatrowski G, Baldomir D, Warda K, Pereiro M, Wojczak L and Arias J E 2004 *J. Magn. Magn. Mater.* **277** 285
[23] Moutie A and Kerouad M 2001 *M. J. Condens. Matter* **4** 77
[24] Jascur M and Kaneyoshi T 1993 *J. Phys.: Condens. Matter* **5** 6313
[25] Kaneyoshi T 1995 *Phys. Rev.* B **52** 7304
[26] Bengrine M, Benyoussef A, El Kenz A, Mhirech F and Peliti L 1999 *Physica* B **269** 34
[27] Jascur M and Kaneyoshi T 1995 *Physica* A **220** 542
[28] Kaneyoshi T 1994 *J. Phys.: Condens. Matter* **6** 10691
[29] Bentaleb M, El Aouad N and Saber M 2002 *Phys. Status Solidi* b **231** 529
[30] Kaneyoshi T 1999 *J. Phys.: Condens. Matter* **11** 7311
[31] Jascur M and Kaneyoshi T 1997 *J. Magn. Magn. Mater.* **168** 47
[32] Htoutou K, Ainane A and Saber M 2004 *J. Magn. Magn. Mater.* **269** 245
[33] Jiang W, Wei G-Z and Du A 2002 *J. Magn. Magn. Mater.* **250** 49
[34] Bengrine M, Benyoussef A, El Kenz A, Loulidi M and Mhirech F 1998 *J. Magn. Magn. Mater.* **183** 334
[35] Hu C-K, Izmailian N Sh and Oganesyan K B 1999 *Phys. Rev.* E **59** 6489
[36] Leita V S, Godoy M and Figueiredo W 2005 *Phys. Rev.* B **71** 094427
[37] Chern G, Horng L, Shieh W K and Wu T C 2001 *Phys. Rev.* B **63** 094421
[38] Ananikian N S, Izmailian N Sh and Oganessyan K A 1998 *Physica* A **254** 207
[39] Albayrak E 2003 *Phys. Status Solidi* b **239** 411
[40] Bobák A 1998 *Physica* A **258** 140
[41] Schmittmann B and Zia R K P 1998 *Phys. Rep.* **301** 45